

PVT: Point-Voxel Transformer for 3D Deep Learning

Cheng Zhang^{1*}, Haocheng Wan^{1*}, Shengqiang Liu¹, Xinyi Shen², Zizhao Wu^{1†}

¹Hangzhou Dianzi University ²University College London
Hangzhou, China 310000
zhangcheng828@hdu.edu.cn

Abstract

In this paper, we present an efficient and high-performance neural architecture, termed Point-Voxel Transformer (PVT) for 3D deep learning, which deeply integrates both 3D *voxel*-based and *point*-based self-attention computation to learn more discriminative features from 3D data. Specifically, we conduct multi-head self-attention (MSA) computation in *voxels* to obtain efficient learning pattern and the coarse-grained local features while performing self-attention in *points* to provide finer-grained information about the global context. In addition, to reduce the cost of MSA computation but achieve high efficiency, we design a *cyclic shifted boxing scheme* by limiting the MSA computation to non-overlapping local box and also preserving cross-box connection. Evaluated on classification benchmark, our PVT not only achieves state-of-the-art accuracy of 94.0% (no voting) but outperforms previous Transformer-based models with $7\times$ measured speedup on average. On part and semantic segmentation, our model also obtains strong performance (86.5% and 68.2% mIoU, respectively). For 3D object detection task, we replace the primitives in Frustrum PointNet with PVT layer and achieve an improvement of 8.6% AP.

1 Introduction

3D deep learning has been receiving increasing attention from both industry and academia thanks to its wide applications including autonomous driving, robotics, AR/VR, etc. In these settings, sensors like LIDAR produce irregular and unordered sets of points that correspond to object surfaces. Yet how to correctly and quickly classify each point from this data remains a challenging problem for 3D deep learning.

Most existing 3D learning methods could be classified into two categories in terms of data representations, i.e., the *voxel*-based models and the *point*-based models. The *voxel*-based models are generally rasterize point clouds onto regular grids and apply 3D convolution for feature learning (Zhou and Tuzel 2018; Qi et al. 2016; Wang and Lu 2019). These models are computationally efficient due to their excellent memory locality, but the inevitable information loss degrades the fine-grained localization accuracy (Shi et al.

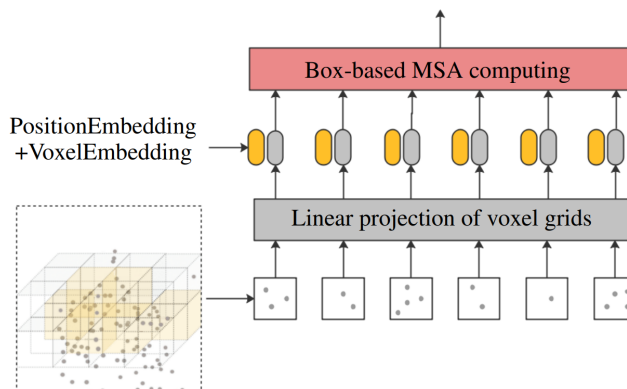


Figure 1: The *voxel*-based branch: we convert point cloud into fixed-size voxel grids, linearly embed each of them, add position embeddings, and feed the resulting sequence of vectors to a B-MSA computing module.

2019). In contrast, The *point*-based models naturally preserve accurate point location, but are generally computationally intensive. (Wang, Samari, and Siddiqi 2018; Chen et al. 2020; Lan et al. 2019). Powered by Transformer (Vaswani et al. 2017) and its variants (Liu et al. 2021a; Dosovitskiy et al. 2021), the *point*-based models have recently applied self-attention (the core unit of Transformer) to extract features from point clouds and obtained significant performance improvement (Guo et al. 2021; Engel et al. 2020; Zhao et al. 2021; Yan et al. 2020). These Transformer-based models can achieve larger receptive field by the self-attention operator but have higher computation cost since they waste a high percentage of their runtime on structuring the irregular and sparse data, instead of being spent on the actual feature learning (Liu et al. 2019b).

Generally, the *voxel*-based models have regular data locality and can efficiently encode coarse-grained features, while the *point*-based networks preserve accurate location information with the flexible fields and can effectively aggregate fine-grained features. In this paper, we focus on how to fully exploit the potential of the two types of methods in Transformer architecture while avoiding their shortcomings, so as to capture more discriminative features from 3D data.

To investigate this, we behave multi-head self-attention

*These authors contributed equally.

†Corresponding author.

(MSA) computation in *voxels* to obtain efficient learning pattern while conducting self-attention in *points* to preserve accurate location information with the flexible fields. However, major challenge is that the global-MSA computation leads to quadratic complexity with respect to the number of voxel grids, making it unsuitable for many 3D vision tasks such as semantic segmentation that require dense prediction or to represent a high-resolution voxels. To tackle this issue, we design a Box-based MSA (B-MSA) computing method which only has linear computational complexity by computing MSA locally within non-overlapping box. A key design element of B-MSA lies in its *cyclic shift* of the box partition between consecutive MSA layers (see Figure 3), which introducing cross-box connections while maintaining the efficient computation of B-MSA.

We propose Point-Voxel Transformer (PVT) with two-branch strategy which mainly consists of the *voxel*-based branch and the *point*-based branch (see Figure 2). As illustrated in Figure 5, by behaving B-MSA in the *voxel*-based branch and performing self-attention in the *point*-based branch, our PVT disentangles the coarse-grained local feature aggregation and the fine-grained global context transformation so that each branch can be implemented efficiently and effectively.

Extensive experiments have demonstrated that our PVT achieves strong performance on the recognition tasks of object classification, semantic segmentation and 3D object detection. Specifically, we perform the classification task on the ModelNet40 and achieve the strong accuracy of 94.0% (no voting), while being on average $7\times$ faster than previous Transformer-based models. On ShapeNet and S3DIS datasets, our model also obtains comparable performance (86.5% and 68.2% mIoU, respectively). For 3D object detection task, we replace the primitives in Frustum PointNet with PVT layer and achieve the improvement of 8.6% AP on the *val set* of KITTI.

The main contributions are summarized as following:

- We propose an efficient and high-performance 3D architecture, termed Point-Voxel Transformer, which deeply incorporating the advantages from both *point*-based and *voxel*-based networks.
- We design a novel *voxel*-based local feature encoding method, which has linear computational complexity and can be extended to any other 3D learning framework.
- Extensive experiments demonstrate that the PVT achieves strong performance on general 3D tasks with $7\times$ speed-up than previous Transformer-based models.

2 Related Works

2.1 Voxel-based 3D models

To extend the success of convolutional neural networks on images, researchers endeavor to transfer point clouds directly to the occupancy grid and apply 3D convolution for feature learning (Choy, Gwak, and Savarese 2019; Le and Ye 2018). However, the memory and computational consumption of such full-voxel-based models increases cubically with respect to the voxel’s resolution. To overcome the

above issue, O-CNN (Wang et al. 2017), OctNet (Riegler, Ulusoy, and Geiger 2016) and kd-Net (Klokov and Lempitsky 2017) are proposed to construct tree structures for occupied voxels so as to discard the computation in the empty grids. Although Octree-based methods are efficient in data structuring, there will be information loss during voxelization since multiple bucketing points into the same voxel grid will lead to indistinguishable of features for learning.

Compared with most *voxel*-based 3D models, our PVT is more efficient and effective: 1) instead of using 3D convolutions, our *voxel*-based feature encoding method directly performs Box-based MSA computation which has linear computational complexity with respect to voxel resolution. 2) as we employ self-attention in the *point* domain, an inherent advantage is that we are able to maintain the same number of points and avoid feature loss during voxelization.

2.2 Point-based 3D models

Instead of voxelization, it is possible to make a neural network that consumes directly on point clouds. Qi et al. proposed PointNet, the pioneering work that learns directly on sparse and unstructured point clouds. Inspired by PointNet, many recent works introduced sophisticated neural modules to learn per-point features. These models can be generally classified as: 1) neighbouring feature pooling (Zhao et al. 2019a; Huang, Wang, and Neumann 2018), 2) graph message passing (Wang et al. 2018b; Zhang et al. 2019; Wang et al. 2019), and 3) attention-based or Transformer-based models (Shi et al. 2021; Zhang and Xiao 2019; Yang et al. 2019; Guo et al. 2021; Zhao et al. 2021; Engel et al. 2020).

Due to the sparsity and irregularity of the point cloud data, methods that directly consume points have achieved state-of-the-art performance. However, the cost of data structuring has become the computation burden on large-scale point clouds (Liu et al. 2019b; Xu et al. 2020).

2.3 Self-attention and Transformer in NLP and CV

(Bahdanau et al. 2014) proposed a neural machine translation method with an attention mechanism, in which attention weight is computed through the hidden state of an RNN. Then Lin et al. further proposed self-attention to visualize and interpret sentence embeddings. Subsequent works employed self-attention layers to replace some or all of the spatial convolution layers. For example, Vaswani et al. proposed Transformer for machine translation. Devlin et al. proposed bidirectional transformers (BERT), which is one of the most powerful models in the NLP field.

Witness the success of self-attention and Transformer architectures in NLP, researchers applied them to vision tasks (Hu et al. 2019; Ramachandran et al. 2019; Zhao, Jia, and and 2020). For instance, Dosovitskiy et al. proposed an image recognition network, ViT, which directly applied a Transformer architecture on image patches and achieved better performance than the traditional convolutional neural networks. Liu et al. recently introduced Swin Transformer to incorporate inductive bias for spatial locality, as well as for hierarchy and translation invariance.

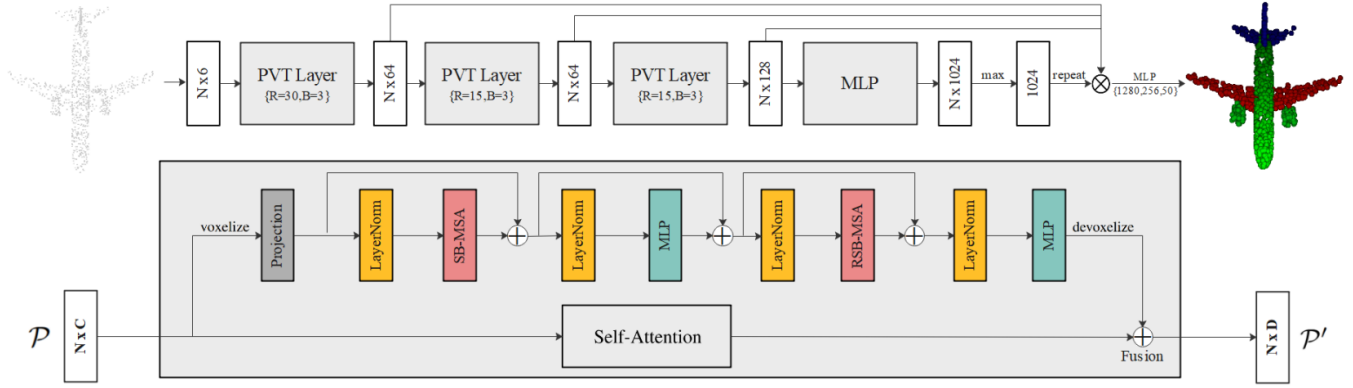


Figure 2: **Model Architecture:** The model for part segmentation take as input N points and feeds them into 3 stacked PVT layers to learn a semantically rich and discriminative representation for each point, followed by a MLP layer to generate the output feature. After that, we leverage the max-pooling and repeating operators to extract an effective global feature representing the entire point cloud. Note that shortcut connections are used to extract multi-scale features and one MLP layer (1280) to aggregate multi-scale features, where we concatenate features from previous layers to get a $64+64+128+1024=1280$ dimensional point cloud. Finally, we predict the final point-wise segmentation scores for the input point cloud and the part label of a point is also determined as the one with maximal score. **PVT layer:** The PVT layer (grey box) is composed of two branches. The upper branch is *voxel*-based for aggregating local features and the lower is *point*-based for capturing global features. We can effectively fuse two branches because they are providing complementary information. R and B denote the voxel resolution size and box size, respectively. \oplus : addition, \otimes : concatenation.

Inspired by above works, we present a Transformer-based neural architecture for 3D deep learning. Extensive experiments have verified its effectiveness and efficiency.

3 Method

Overview

In contrast to the previous Transformer-based 3D models, the main goal of our network is to make the model as efficient as possible so that it can be widely used and ensure the high accuracy on various 3D tasks at the same time.

We introduce an efficient and high-performance method for 3D deep learning: Point-Voxel Transformer(PVT). Formally, given a point cloud $\mathcal{P} \in \mathbb{R}^{N \times C}$, our PVT layer is designed to map the input features \mathcal{P} to a new set of point feature $\mathcal{P}' \in \mathbb{R}^{N \times D}$. As illustrated in Figure 2, the PVT layer consists of two main branches: a *voxel*-based branch and a *point*-based branch. We leverage the *voxel*-based branch to map the inputs \mathcal{P} to $\mathcal{P}_{local} \in \mathbb{R}^{N \times D}$ which aggregates local features in the *voxel* domain, and bypasses expensive operators. However, full *voxel*-based method will inevitably encounter information loss during voxelization. Thus, we utilize the *point*-based branch to map the inputs \mathcal{P} to $\mathcal{P}_{global} \in \mathbb{R}^{N \times D}$ that directly extracts global features for each individual point. With both local features and aggregated global context, we can efficiently fuse two branches with an addition layer as both of them provide complementary information.

Below we detail the *voxel*-based and the *point*-based branches in Section 3.1 and 3.2 respectively. Section 3.3 details our feature fusion module. Finally, Section 3.4 discusses the relationship between the proposed method and the prior works.

3.1 The Voxel-based Branch

This branch aims to effectively capture local information, which can bypass expensive sampling and neighbor points querying. Specifically, it contains three steps: voxelization, feature aggregation and devoxelization.

Akin to PVCNN (Liu et al. 2019b), we use the same voxelized and devoxelized methods, which map the input point cloud \mathcal{P} to a new set of voxel features V and transform the voxel-wise features back to the point-wise features \mathcal{P}_{local} . Unlike PVCNN, we apply the standard Transformer architecture to perform feature aggregation on regular 3D grids, which brings us with significant improvement of accuracy. However, the global-MSA of Transformer leads to quadratic complexity with respect to the number of voxels, since the relationships between a voxel and all other voxels are measured.

Box-based MSA: To obtain efficient modeling power, we propose to compute MSA within local boxes, which are arranged to evenly partition the voxel space in a non-overlapping manner. Assume that each local box contains $B \times B \times B$ voxel grids and R denotes the voxel resolution, the computational complexity of a global MSA and a Box-based one on R^3 voxel grids are:

$$\Omega(\text{Global-MSA}) = 4R^3 D^2 + 2(R^3)^2 D \quad (1)$$

$$\Omega(\text{B-MSA}) = 4R^3 D^2 + 2B^3 R^3 D \quad (2)$$

where the former is quadratic to voxel grids number R^3 , and the latter is linear when B is fixed, D is the dimension of features. In summary, global-MSA computation is generally unaffordable for a large voxel resolution, while the local B-MSA is scalable.

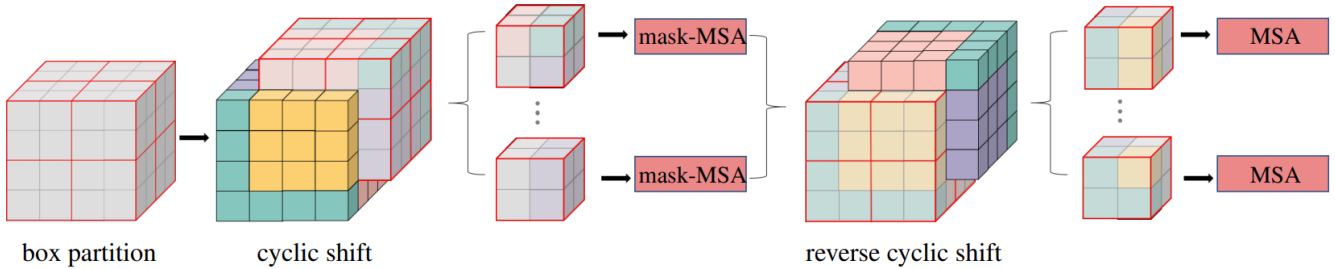


Figure 3: Illustration of the MSA computing in *cyclic shifted box* partitioning. In this example, $R=4$, $B=2$. First, we chop up the entire voxel grids into a $(2,2,2)$ tensor of non-overlapping $(2,2,2)$ boxes. Second, by cyclic-shifting toward the down-left-front direction, a batched box may be composed of several sub-boxes that are not adjacent in the feature map, thus we employ a masking-MSA within each box. Finally, we perform MSA computing in each local box after reverse cyclic-shifting. Readers can refer to our supplementary video for more details.

Cyclic shifted box partitioning method: The B-MSA lacks information interaction across boxes, which may limit the representation power of PVT. Thus, we extend the shifted 2D window mechanism of Swin Transformer (Liu et al. 2021a) to 3D boxes for the purpose of introducing cross-box information interaction while maintaining the efficient computation of non-overlapping box based MSA.

Figure 3 depicts the different steps involved in executing *cyclic shifted box* based MSA for voxel grids with resolution $R = 4$ and $B = 2$. The MSA module in the first layer uses the regular box partition strategy such that we obtain $(2, 2, 2)$ non-overlapping boxes. Then, the next module adopts a boxing configuration that is shifted from that of the preceding layer, by cyclic-shifting toward down-left-front direction from the regularly partitioned boxes. After that, a batch box may be composed of several sub-boxes that are not adjacent in the feature map, so we adopt a masking mechanism to limit MSA computation to within each sub-boxes. Finally, after reverse cyclic shifting, each box behaves a local MSA computation.

With the *cyclic shifted box* partitioning approach, The step of feature aggregation can be described as:

$$V^\ell = SB\text{-MSA}(LN(V^{\ell-1})) + V^{\ell-1} \quad (3)$$

$$\hat{V}^\ell = MLP(LN(V^\ell)) + V^\ell \quad (4)$$

$$V^{\ell+1} = RSB\text{-MSA}(LN(\hat{V}^\ell)) + \hat{V}^\ell \quad (5)$$

$$\hat{V}^{\ell+1} = MLP(LN(V^{\ell+1})) \quad (6)$$

where V^ℓ and \hat{V}^ℓ denote the output features of the SB-MSA module and the MLP module for layer ℓ , respectively; SB-MSA and RSB-MSA denote MSA computation using shifted and reverse shifted box partitioning configurations, respectively.

In general, it is important to note that with the *cyclic shifted box* partitioning approach, the *voxel*-based branch introduces information interaction between neighboring non-overlapping boxes and is suitable for 3D vision problems such as shape classification, semantic segmentation and 3D object detection.

	Layer Type	Time Complexity per Layer
Voxel-based	3D Convolutions	$\mathcal{O}(k \cdot R^3 \cdot D^2)$
	B-MSA	$\mathcal{O}(v \cdot R^3 \cdot D)$
Point-based	1D Convolutions	$\mathcal{O}(k \cdot N \cdot D^2)$
	Global-SA	$\mathcal{O}(N^2 \cdot D)$

Table 1: Per-layer complexity for different layer types. R is the resolution of voxels, v is number of voxel grids in a same box, N is the number of points, D is the representation dimension and k is the kernel size of convolutions.

3.2 The Point-based Branch

The *voxel*-based branch gathers the neighborhood information with low-resolution. However, in order to capture long-range dependencies, low-resolution *voxel*-based branch alone is limited. To this end, we directly employ self-attention on the entire point cloud for global context aggregation. The *point*-based branch is computed as:

$$\mathcal{P}_{sa} = softmax(Q \cdot K^T) \cdot V, \quad \mathcal{P}_{sa} \in \mathbb{R}^{N \times D} \quad (7)$$

$$\mathcal{P}_{global} = MLP(\mathcal{P}_{sa}) + \mathcal{P}_{in}, \quad \mathcal{P}_{global} \in \mathbb{R}^{N \times D} \quad (8)$$

where $(Q, K, V) \in \mathbb{R}^{N \times D}$ is generated by shared linear transformations and the input features \mathcal{P}_{in} , they are all ordered independent. Moreover, *softmax* and *weighted sum* are both permutation-independent operators. Thus, the standard self-attention computation is permutation-invariant, making it well-suited to handle the irregular, disordered 3D points.

3.3 Feature Fusion

We effectively fuse the outputs of two branches with an addition to combine the complementary information provided.

$$\mathcal{P}' = \mathcal{P}_{local} + \mathcal{P}_{global}, \quad \mathcal{P}' \in \mathbb{R}^{N \times D} \quad (9)$$

3.4 Relationship to prior works

The proposed PVT model is related to several prior works which includes PVCNN (Liu et al. 2019b), PCT (Guo et al. 2021), PT¹ (Engel et al. 2020), PT² (Zhao et al. 2021),.

Although we are inspired by the idea of PVCNN (Liu et al. 2019b), our PVT is different: 1) in the *voxel*-based

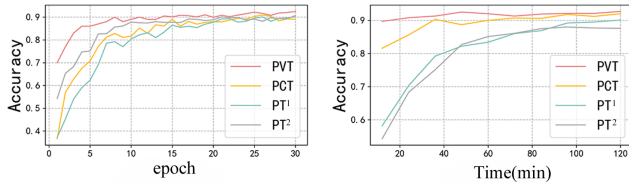


Figure 4: The accuracy of different Transformer-based methods over time and epochs on ModelNet40. In both equal-time and equal-epoch comparisons, our method performs the best. The accuracy of 90% can be achieved not only after 8 epochs but also in the shortest training time.

branch, PVCNN uses a 3D convolution to gather local information while we employ MSA computation within each local box, which is more efficient (see Table 1, $k \cdot D > v$. v is 64 and D is 128 in our settings. In PVCNN’s setting, the kernel size k is 3). 2) in the *point*-based branch, PVCNN uses a 1D convolution which is computation efficient but lacks the global context modeling capability. By performing self-attention computation on the entire points, our method gathers the global modeling power.

Unlike prior Transformer-based 3D models which need to gather the downsampled points and find the correspond neighbors by using expensive FPS and k -NN in *point* domain, our approach does not require explicitly identify which point is the farthest and what are in the neighboring set. Instead, the *voxel*-based branch observes regular data and learns to capture local features using B-MSA. Additionally, the *point*-based branch only needs to perform self-attention on the entire point cloud, which also does not require to find the neighboring points. Thus, our PVT is more efficient than PCT, PT¹ and PT².

4 Experiments and Evaluation

In this section, we evaluate the proposed PVT for different 3D tasks: shape classification, object part segmentation, scene segmentation and 3D object detection. The performance is quantitatively evaluated with four metrics, including overall accuracy (OA), average precision (AP), the intersection over union (IoU), and mean IoU (mIoU). For fair comparison, we report the measured latency on a RTX 2080 GPU to reflect the efficiency but evaluate other indicators on a RTX 3090 GPU. Please refer to our appendices for more detailed experimental settings and results.

Model: The architecture used for the segmentation task is shown in Figure 2. In our settings, dropout with keep probability of 0.5 is used in the last two MLP layers, All layers include ReLU and batch normalization. In addition, for other 3D tasks, we use the similar architecture as in segmentation.

4.1 Shape Classification

We evaluate our model on the ModelNet40 (Wu et al. 2014) dataset. This dataset contains 12,311 CAD models from 40 man-made object categories, in which 9,843 models are used for training and 2468 models are for testing. We follow the

Model	Input	points	OA	Latency
OA < 92.5				
PointNet	xyz	16 × 1024	89.2	13.6
PointNet++	xyz,nor	16 × 1024	91.9	35.3
SO-Net 2018	xyz,nor	8 × 2048	90.9	—
PointGrid 2018	xyz,nor	16 × 1021	92.0	—
SpiderCNN 2018	xyz,nor	8 × 1024	92.4	82.6
PointCNN 2018	xyz	16 × 1024	92.2	221.2
PointWeb 2019b	xyz,nor	16 × 1024	92.3	—
PVCNN 2019b	xyz,nor	16 × 1024	92.4	24.2
OA > 92.5				
KPCConv 2019	xyz	16 × 6500	92.9	120.5
DGCNN 2018b	xyz	16 × 1024	92.9	85.8
LDGCNN 2019	xyz	16 × 1024	92.7	—
PointASNL 2020	xyz,nor	16 × 1024	93.2	923.6
PT ¹ 2020	xyz,nor	16 × 1024	92.8	320.6
PT ² 2021	xyz,nor	8 × 1024	93.7	530.2
PCT 2021	xyz	16 × 1024	93.2	92.4
PVT (Ours)	xyz	16 × 1024	93.6	45.5
PVT (Ours)	xyz,nor	16 × 1024	94.0	48.6

Table 2: Results on ModelNet40 (Wu et al. 2015). Compared with previous Transformer-based models, our PVT achieves the state-of-the-art accuracy with 7 × measured speed-up on average.

experimental configuration of PointNet, i.e., for each model, we uniformly sample 1024 points from the mesh faces; the point cloud is re-scaled to fit the unit sphere.

Results. In Table 2, we can see our PVT outperforms most previous models. PVT directly improves the accuracy of its backbone (PointNet) by 4.8%. Remarkably, compared with previous Transformer-based models, such as PCT, PT¹ and PT², our PVT not only achieves strong accuracy of 94.0%, but has the best speed-accuracy trade-off (7 × faster on average). In addition, Figure 4 provides an accuracy plot under equal-epoch setting. As can be seen, our method outperform all Transformer-based methods, being the fastest and most accurate towards convergence.

4.2 Object Part Segmentation

We evaluate our model on ShapeNet Parts (Wu et al. 2014). The ShapeNet Parts contains a total of 16,880 models (14,006 models are used for training, 2874 models for testing), each of which is annotated with two to six parts and the entire data set has 50 different part labels. We sample 2048 points from each model as input, in which few point sets have six labeled parts. We directly adopt the same train-test split as PointNet in our experiment.

Results. Table 3 shows the class-wise segmentation results. The results show that our PVT (86.5% pIoU) makes an improvement of 2.8% over PointNet and outperforms previous Transformer-based models.

Visualization. In Figure 5, We illustrate output features from the *point*-based and *voxel*-based branches respectively, where warmer color represents larger magnitude. As we can see, the *voxel*-based branch captures large, continuous parts

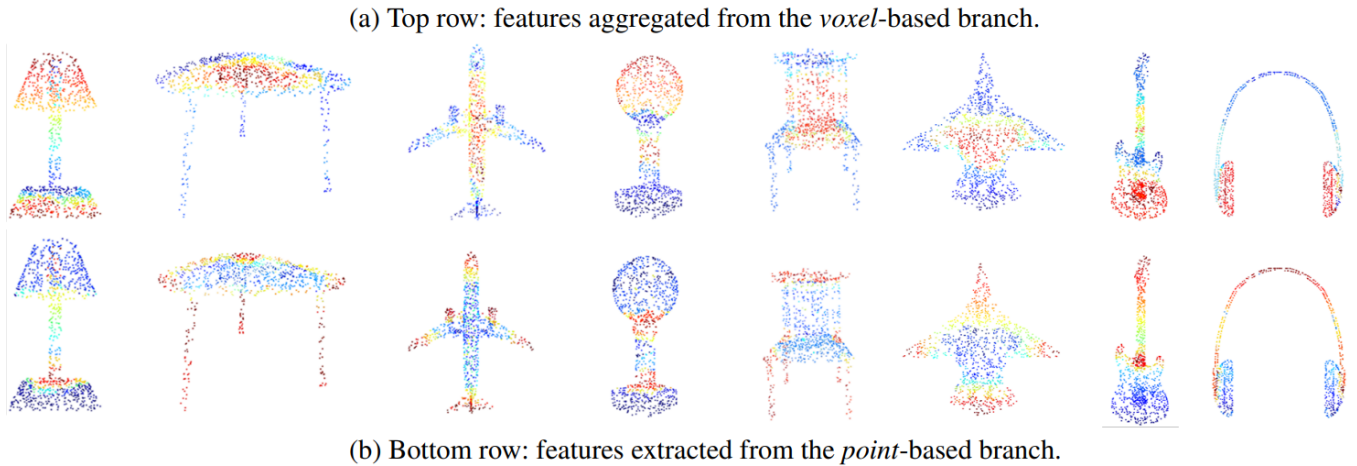


Figure 5: We demonstrate the output features extracted from two branches using Open3D (Zhou, Park, and Koltun 2018). The *voxel*-based branch focuses on the large, continuous parts, while the *point*-based captures the global shape details.

Model	pIoU	Areo	Bag	Cap	Car	Chair	Ear Phone	Guitar	Knife	Lamp	Laptop	Motor	Mug	Pistol	Rocket	Skate Board	Table
# Shapes		2690	76	55	898	3758	69	787	392	1547	451	202	184	283	66	152	5271
PointNet	83.7	83.4	78.7	82.5	74.9	89.6	73.0	91.5	85.9	80.8	95.3	65.2	93.0	81.2	57.9	72.8	80.6
P2Sequence2018	85.1	82.6	81.8	87.5	77.3	90.8	77.1	91.1	86.9	83.9	95.7	70.8	94.6	79.3	58.1	75.2	82.8
PointASNL	86.1	84.1	84.7	87.9	79.7	92.2	73.7	91.0	87.2	84.2	95.8	74.4	95.2	81.0	63.0	76.3	83.2
RS-CNN 2019a	86.2	83.5	84.8	88.8	79.6	91.2	81.1	91.6	88.4	86.0	96.1	73.7	94.1	83.4	60.5	77.7	83.6
PT ¹	85.9	—	—	—	—	—	—	—	—	—	—	—	—	—	—	—	—
PCT	86.4	85.0	82.4	89.0	81.2	91.9	71.5	91.3	88.1	86.3	95.8	64.6	95.8	83.6	62.2	77.6	73.7
PVT (Ours)	86.5	85.1	82.8	88.3	81.5	92.2	72.5	91.0	88.9	85.6	95.4	76.2	94.7	84.2	65.0	75.3	81.7

Table 3: Results of part segmentation on ShapeNet. pIoU means part-average Intersection-over-Union.

Model	mIoU	Ceiling	Floor	Wall	Bean	Column	Window	Door	Chair	Table	Bookcase	Sofa	Board	Clutter
PointNet	41.09	88.80	97.33	69.80	0.05	3.92	46.26	10.76	52.61	58.93	40.28	5.85	26.38	33.22
PointNet++	50.04	90.79	96.45	74.12	0.02	5.77	43.59	25.39	69.22	76.94	21.45	55.61	49.34	41.88
DGCNN	47.08	92.42	97.46	76.03	0.37	12.00	51.59	27.01	64.85	68.58	7.67	43.76	29.44	40.83
PVCNN	56.12	91.23	97.54	77.13	0.29	13.02	51.72	26.74	68.52	75.48	28.64	53.29	27.21	41.92
BPM 2021	61.43	—	—	—	—	—	—	—	—	—	—	—	—	—
IAF-Net 2021	64.60	91.41	98.60	81.80	0.00	34.90	62.00	54.70	79.70	86.90	49.90	72.40	74.80	52.10
PVT(Ours)	65.30	91.18	98.76	86.23	0.31	34.21	49.90	61.45	81.62	89.85	48.20	79.96	76.45	54.67

Table 4: Indoor scene segmentation results on the S3DIS dataset, evaluated on Area5. From this table, we can see that the proposed PVT outperforms most of previous 3D models in all categories significantly,

	LBE	mAP	Car			Predestrian				Cyclist		
			Easy	Mod.	Hard	Easy	Mod.	Hard	Easy	Mod.	Hard	
F-PointNet (Qi et al. 2017b)	✗	63.16	83.26	69.28	62.56	65.08	55.85	49.28	74.54	55.95	52.65	
F-PointNet++ (Qi et al. 2017b)	✓	65.58	83.76	70.92	63.65	70.02	61.32	53.51	77.15	56.49	53.37	
F-PVCNN (Liu et al. 2019b)	✗	65.68	84.22	71.11	63.63	69.16	60.28	52.32	78.37	57.59	54.06	
F-PVT (Ours)	✗	66.93	85.75	73.58	65.12	68.54	60.36	52.85	80.57	59.40	56.18	

Table 5: Results of 3D object detection on the *val* set of KITTI. Our PVT outperforms F-PVCNN in all categories significantly, ALB means that aggregating local features in the box estimation network.

Model	mIoU(%)	OA(%)	mAcc(%)
PointNet	47.6	78.5	66.2
G+RCU 2017	49.7	81.1	—
TangentConv 2018	52.8	—	—
RSNet 2018	56.5	—	66.5
3P-RNN 2018	56.3	86.9	—
SGPN 2018a	50.4	—	—
SPGraph 2018	62.1	85.5	73.0
PVCNN	63.2	85.8	72.5
ShellNet 2019	66.8	87.1	—
PVT(Ours)	68.2	87.3	75.0

Table 6: Results of semantic segmentation of 3D indoor scenes on S3DIS, evaluated with 6-fold cross-validation. From this table, we can see that the proposed PVT outperforms most of previous 3D models.

while the *point*-based counterpart captures global shape details (e.g., table legs, airplane wings and tail).

4.3 Indoor Scene Segmentation

We evaluate our model on S3DIS dataset (Armeni et al. 2017), which contains 3D RGB point clouds from six indoor areas of three different buildings. Each point is marked with a semantic label from 13 categories—e.g. board, bookcase, chair, ceiling, and beam—plus clutter. We follow Tchapmi et al. and Qi et al. and divide each room into $1m \times 1m$ blocks, where each point is represented by a 9-dimensional vector (XYZ, RGB, and normalized spatial coordinates).

Results. The results are presented in Table 4 and 6. On Area 5, the PVT improves its backbone (PointNet) by 24.2% in mIoU, and it also outperforms PVCNN by a large margin in accuracy. Moreover, PVT attains mIoU of 68.2% under 6-fold cross-validation, substantially outperforming most prior models.

4.4 3D Object Detection

We finally conduct experiments on the driving-oriented dataset, KITTI (Geiger et al. 2013). We follow (Qi et al. 2017b) to construct the *val set* from the training set so that no instances in the *val set* belong to the same video clip of any training instance. The size of *val set* is 3769, leaving the other 3711 samples for training. We have evaluated all models for 20 times per each dataset and reported the mean 3D AP.

Results. In Table 5, even if our model does not aggregate neighboring features in the box estimation network while F-PointNet++ does, ours still outperform it in most classes. Compared with F-PointNet baseline, our PVT obtains up to 5% mAP improvement in pedestrians and 3.53-6.03% mAP improvement in cyclist, which indicates that the proposed PVT is both efficient and expressive.

5 Ablation Studies

In this section, we conduct extensive ablation study to analyze the effectiveness of different components of PVT. All

Model	PB	VB	shifting	NPL	OA	Latency
A	✗	✓	✓	3	92.8	33.5
B	✓	✗	✓	3	92.3	25.2
C	✓	✓	✗	3	93.0	47.9
D	✓	✓	✓	2	93.1	36.4
E	✓	✓	✓	4	93.6	72.5
PVT ^{full}	✓	✓	✓	3	94.0	48.6

Table 7: Ablation study on ModelNet40. PB and VB mean the *point*-based branch and the *voxel*-based branch; NPL denotes the number of PVT layers; shifting means all self-attention modules adopt the *cyclic shifted box* partitioning method.

experiments are trained on the shape classification. The results of the ablation study are summarized in Table 7.

Impact of the voxel-based and point-based branches.

We set two baselines: A and B. Model A only encodes global context features by the *point*-based branch, and Model B only encodes local features by the *voxel*-based one. As reported in Table 7, the Baseline model A gets a low accuracy of 92.8% on classification benchmarks, and model B gets 92.3%. When we combine local and global features (PVT^{full}), there is a notable improvement in both tasks. This means our network can take advantage of the combination of two branches, which provides richer information about the points.

Effect of the cyclic shifted boxes scheme. Ablation of the *shifted box* method on classification are reported in Table 7 (Model C). PVT with the *shifted box* partitioning outperforms the counterpart build on a single box at each layer by +1.2 OA on ModelNet40. The results indicate the effectiveness and efficiency of using *cyclic shifted boxes* to build cross-box information interaction in the preceding layers.

Impact of the number of PVT layer. we validate the impact of the PVT layer by controlling the number of PVT layers and report the results in Table 7. From this table we can conclude the following: on one hand, reducing the number of PVT layer can save latency, for example, compare with PVT^{full}, Model D saves 25% latency but incurs a loss on accuracy; on the other hand, increasing the number of PVT layer from PVT^{full} can hardly support Model E accuracy benefit but leads to an increase on latency. To balance between speed and accuracy, we set 3 PVT layers as our full model.

6 Conclusion and Future Work

In this paper, we present a pure-transformer backbone architecture for 3D deep learning that is found to surpass previous Transformer-based models in performance and efficiency. It achieves this by deeply combining the advantages from both the *voxel*-based and the *point*-based networks. In addition, to reduce the computation cost, we design a *cyclic shifted box* based MSA computing method which has linear computational complexity with respect to voxel resolution.

In the future, we expect to promote the primary structure for other research areas, such as point cloud generation and completion.

References

- Armeni, I.; Sax, S.; Zamir, A. R.; and Savarese, S. 2017. Joint 2D-3D-Semantic Data for Indoor Scene Understanding. *CoRR*, abs/1702.01105.
- Bahdanau; Dzmitry; Cho, K.; and Bengio, Y. 2014. Neural machine translation by jointly learning to align and translate. in *ICLR*.
- Chen, C.; Li, G.; Xu, R.; Chen, T.; Wang, M.; and Lin, L. 2020. ClusterNet: Deep Hierarchical Cluster Network With Rigorously Rotation-Invariant Representation for Point Cloud Analysis. *2019 IEEE/CVF Conference on Computer Vision and Pattern Recognition (CVPR)*.
- Choy, C.; Gwak, J. Y.; and Savarese, S. 2019. 4D Spatio-Temporal ConvNets: Minkowski Convolutional Neural Networks. *2019 IEEE/CVF Conference on Computer Vision and Pattern Recognition (CVPR)*.
- Devlin, J.; Chang, M. W.; Lee, K.; and Toutanova, K. 2018. BERT: Pre-training of Deep Bidirectional Transformers for Language Understanding. in *NAACL-HLT*.
- Dosovitskiy, A.; Beyer, L.; Kolesnikov, A.; Weissenborn, D.; Zhai, X.; Unterthiner, T.; Dehghani, M.; Minderer, M.; Heigold, G.; Gelly, S.; Uszkoreit, J.; and Houslyby, N. 2021. An Image is Worth 16x16 Words: Transformers for Image Recognition at Scale. *ICLR*.
- Engel, N.; Belagiannis, V.; Dietmayer, K.; and zhang cheng. 2020. Point Transformer. *CoRR*, abs/2011.00931.
- Engelmann, F.; Kontogianni, T.; Hermans, A.; and Leibe, B. 2017. Exploring Spatial Context for 3D Semantic Segmentation of Point Clouds. *2017 IEEE International Conference on Computer Vision Workshop (ICCVW)*.
- Geiger, A.; Lenz, P.; Stiller, C.; and Urtasun, R. 2013. Vision meets robotics: The KITTI dataset. *International Journal of Robotics Research*, 32(11): 1231–1237.
- Gong, J.; Xu, J.; Tan, X.; Zhou, J.; Qu, Y.; Xie, Y.; and Ma, L. 2021. Boundary-Aware Geometric Encoding for Semantic Segmentation of Point Clouds. *Proceedings of the AAAI Conference on Artificial Intelligence*.
- Guo, M.-H.; Cai, J.-X.; Liu, Z.-N.; Mu, T.-J.; Martin, R. R.; and Hu, S.-M. 2021. PCT: Point cloud transformer. *Computational Visual Media*, 7(2): 187–199.
- Hu, H.; Zhang, Z.; Xie, Z.; and Lin, S. 2019. Local Relation Networks for Image Recognition. in *ICCV*.
- Huang, Q.; Wang, W.; and Neumann, U. a. 2018. Recurrent Slice Networks for 3D Segmentation of Point Clouds. *2018 IEEE/CVF Conference on Computer Vision and Pattern Recognition*.
- Klokov, R.; and Lempitsky, V. 2017. Escape from cells: Deep kd-networks for the recognition of 3d point cloud models. *Proceedings of the IEEE International Conference on Computer Vision*, 863–872.
- Lan, S.; Yu, R.; Yu, G.; and Davis, L. S. 2019. Modeling Local Geometric Structure of 3D Point Clouds Using Geo-CNN. *2019 IEEE/CVF Conference on Computer Vision and Pattern Recognition (CVPR)*.
- Landrieu, L.; and Simonovsky, M. 2018. Large-Scale Point Cloud Semantic Segmentation with Superpoint Graphs. *CVPR 2018*.
- Le, T.; and Ye, D. 2018. PointGrid: A Deep Network for 3D Shape Understanding. *2018 IEEE/CVF Conference on Computer Vision and Pattern Recognition (CVPR)*.
- Li, J.; Chen, B. M.; and Lee, G. H. 2018. SO-Net: Self-Organizing Network for Point Cloud Analysis. in *CVPR*.
- Li, Y.; Bu, R.; Sun, M.; and Chen, B. 2018. PointCNN: Convolution On X-Transformed Points. *Advances in Neural Information Processing Systems (NIPS)*.
- Lin, Z.; Feng, M.; Santos, C. N. d.; Yu, M.; Xiang, B.; Zhou, B.; and Bengio, Y. 2017. A structured self-attentive sentence embedding. *ICLR*.
- Liu, X.; Han, Z.; Liu, Y. S.; and Zwicker, M. 2018. Point2Sequence: Learning the Shape Representation of 3D Point Clouds with an Attention-based Sequence to Sequence Network. in *AAAI*.
- Liu, Y.; Fan, B.; Xiang, S.; and Pan, C. 2019a. Relation-Shape Convolutional Neural Network for Point Cloud Analysis. in *CVPR*.
- Liu, Z.; Lin, Y.; Cao, Y.; Hu, H.; Wei, Y.; Zhang, Z.; Lin, S.; and Guo, B. 2021a. Swin transformer: Hierarchical vision transformer using shifted windows. *arXiv preprint arXiv:2103.14030*.
- Liu, Z.; Ning, J.; Cao, Y.; Wei, Y.; Zhang, Z.; Lin, S.; and Hu, H. 2021b. Video Swin Transformer. *CoRR*, abs/2106.13230.
- Liu, Z.; Tang, H.; Lin, Y.; and Han, S. 2019b. Point-Voxel CNN for Efficient 3D Deep Learning. *Advances in Neural Information Processing Systems (NIPS)*.
- Mehta, R.; and Arbel, T. 2018. RS-Net: Regression-segmentation 3D CNN for synthesis of full resolution missing brain MRI in the presence of tumours. *International Workshop on Simulation and Synthesis in Medical Imaging*, 119–129.
- Qi, C. R.; Su, H.; Mo, K.; and Guibas, L. J. 2017a. Pointnet: Deep learning on point sets for 3d classification and segmentation. *Proceedings of the IEEE conference on computer vision and pattern recognition*, 652–660.
- Qi, C. R.; Su, H.; Niebner, M.; Dai, A.; Yan, M.; and Guibas, L. J. 2016. Volumetric and Multi-View CNNs for Object Classification on 3D Data. in *CVPR*.
- Qi, C. R.; Wei, L.; Wu, C.; Hao, S.; and Guibas, L. J. 2017b. Frustum PointNets for 3D Object Detection from RGB-D Data. in *CVPR*.
- Ramachandran, P.; Parmar, N.; Vaswani, A.; Bello, I.; Levskaya, A.; and Shlens, J. 2019. Stand-Alone Self-Attention in Vision Models. *CoRR*, abs/1906.05909.
- Riegler, G.; Ulusoy, A. O.; and Geiger, A. 2016. OctNet: Learning Deep 3D Representations at High Resolutions. *IEEE Computer Society*.

- Shi, Q.; Anwar, S.; Barnes, N.; and zhang cheng. 2021. Semantic Segmentation for Real Point Cloud Scenes via Bilateral Augmentation and Adaptive Fusion. *in CVPR*.
- Shi, S.; Guo, C.; Jiang, L.; Wang, Z.; Shi, J.; Wang, X.; and Li, H. 2019. PV-RCNN: Point-Voxel Feature Set Abstraction for 3D Object Detection. *Conference on Computer Vision and Pattern Recognition (CVPR)*.
- Tatarchenko, M.; Park, J.; Koltun, V.; and Zhou, Q. Y. 2018. Tangent Convolutions for Dense Prediction in 3D. *in CVPR*.
- Tchapmi, L.; Choy, C.; Armeni, I.; Gwak, J. Y.; and Savarese, S. 2017. SEGCloud: Semantic Segmentation of 3D Point Clouds. *2017 International Conference on 3D Vision (3DV)*.
- Thomas, H.; Qi, C. R.; Deschaud, J. E.; Marcotegui, B.; and Guibas, L. J. 2019. KPConv: Flexible and Deformable Convolution for Point Clouds. *ICCV*.
- Vaswani, A.; Shazeer, N.; Parmar, N.; Uszkoreit, J.; Jones, L.; Gomez, A. N.; Kaiser, L.; and Polosukhin, I. 2017. Attention Is All You Need. *CoRR*, abs/1706.03762.
- Wang, C.; Samari, B.; and Siddiqi, K. 2018. Local Spectral Graph Convolution for Point Set Feature Learning. *in ECCV*.
- Wang, L.; Huang, Y.; Hou, Y.; Zhang, S.; and Shan, J. 2019. Graph Attention Convolution for Point Cloud Semantic Segmentation. *2019 IEEE/CVF Conference on Computer Vision and Pattern Recognition (CVPR)*.
- Wang, P. S.; Liu, Y.; Guo, Y. X.; Sun, C. Y.; and Tong, X. 2017. O-CNN: Octree-based Convolutional Neural Networks for 3D Shape Analysis. *Acm Transactions on Graphics*, 36(4): 72.
- Wang, W.; Yu, R.; Huang, Q.; and Neumann, U. 2018a. Sgpn: Similarity group proposal network for 3d point cloud instance segmentation. *Proceedings of the IEEE Conference on Computer Vision and Pattern Recognition*, 2569–2578.
- Wang, Y.; Sun, Y.; Liu, Z.; Sarma, S. E.; Bronstein, M. M.; and Solomon, J. M. 2018b. Dynamic Graph CNN for Learning on Point Clouds. *ACM Transactions on Graphics*, 38(5).
- Wang, Z.; and Lu, F. 2019. VoxSegNet: Volumetric CNNs for Semantic Part Segmentation of 3D Shapes. *IEEE Transactions on Visualization and Computer Graphics*, 1–1.
- Wu, Z.; Song, S.; Khosla, A.; Tang, X.; and Xiao, J. 2014. 3D ShapeNets for 2.5D Object Recognition and Next-Best-View Prediction. *CoRR*, abs/1406.5670.
- Wu, Z.; Song, S.; Khosla, A.; Yu, F.; Zhang, L.; Tang, X.; and Xiao, J. 2015. 3D ShapeNets: A Deep Representation for Volumetric Shapes. *2015 IEEE Conference on Computer Vision and Pattern Recognition (CVPR)*.
- Xu, M.; Zhou, Z.; Zhang, J.; and Qiao, Y. 2021. Investigate Indistinguishable Points in Semantic Segmentation of 3D Point Cloud. *Proceedings of the AAAI Conference on Artificial Intelligence*, abs/2103.10339.
- Xu, Q.; Sun, X.; Wu, C.-Y.; Wang, P.; and Neumann, U. 2020. Grid-gcn for fast and scalable point cloud learning. *Proceedings of the IEEE/CVF Conference on Computer Vision and Pattern Recognition*, 5661–5670.
- Xu, Y.; Fan, T.; Xu, M.; Long, Z.; and Yu, Q. 2018. SpiderCNN: Deep Learning on Point Sets with Parameterized Convolutional Filters. *ECCV*.
- Yan, X.; Zheng, C.; Li, Z.; Wang, S.; and Cui, S. 2020. PointASNL: Robust Point Clouds Processing using Non-local Neural Networks with Adaptive Sampling. *2020 IEEE/CVF Conference on Computer Vision and Pattern Recognition (CVPR)*.
- Yang, B.; Wang, J.; Clark, R.; Hu, Q.; Wang, S.; Markham, A.; and Trigoni, N. 2019. Learning Object Bounding Boxes for 3D Instance Segmentation on Point Clouds. *2019 IEEE/CVF Conference on Computer Vision and Pattern Recognition (CVPR)*.
- Ye, X.; Li, J.; Huang, H.; Du, L.; and Zhang, X. 2018. 3d recurrent neural networks with context fusion for point cloud semantic segmentation. *Proceedings of the European Conference on Computer Vision (ECCV)*, 403–417.
- Zhang, K.; Hao, M.; Wang, J.; Silva, C. D.; and Fu, C. 2019. Linked Dynamic Graph CNN: Learning on Point Cloud via Linking Hierarchical Features. *arXiv:1904.10014 [cs]*.
- Zhang, W.; and Xiao, C. 2019. PCAN: 3D Attention Map Learning Using Contextual Information for Point Cloud Based Retrieval. *2019 IEEE/CVF Conference on Computer Vision and Pattern Recognition (CVPR)*.
- Zhang, Y.; Li, Z.; Xie, Y.; Qu, Y.; Li, C.; and Mei, T. 2021. Weakly Supervised Semantic Segmentation for Large-Scale Point Cloud. *Proceedings of the AAAI Conference on Artificial Intelligence*, 35(4): 3421–3429.
- Zhang, Z.; Hua, B. S.; and Yeung, S. K. 2019. ShellNet: Efficient Point Cloud Convolutional Neural Networks using Concentric Shells Statistics. *2019 IEEE/CVF International Conference on Computer Vision (ICCV)*.
- Zhao, H.; Jia, J.; and and, V. K. 2020. Exploring Self-attention for Image Recognition. *Conference on Computer Vision and Pattern Recognition (CVPR)*.
- Zhao, H.; Jiang, L.; Fu, C. W.; and Jia, J. 2019a. PointWeb: Enhancing Local Neighborhood Features for Point Cloud Processing. *2019 IEEE/CVF Conference on Computer Vision and Pattern Recognition (CVPR)*.
- Zhao, H.; Jiang, L.; Fu, C.-W.; and Jia, J. 2019b. Pointweb: Enhancing local neighborhood features for point cloud processing. *Proceedings of the IEEE/CVF Conference on Computer Vision and Pattern Recognition*, 5565–5573.
- Zhao, H.; Jiang, L.; Jia, J.; Torr, P.; and Koltun, V. 2021. Point transformer. *arXiv preprint arXiv:2012.09164*.
- Zhou, Q.-Y.; Park, J.; and Koltun, V. 2018. Open3D: A Modern Library for 3D Data Processing. *arXiv:1801.09847*.
- Zhou, Y.; and Tuzel, O. 2018. Voxnet: End-to-end learning for point cloud based 3d object detection. *Proceedings of the IEEE Conference on Computer Vision and Pattern Recognition (ICCV)*, 4490–4499.